DOI: 10.1002/chem.201000728

Surprising Properties of a Furo-Furanone

Gion Calzaferri,*[a] Dominik Brühwiler,*[b] Tao Meng,[a] Le-Quyenh Dieu,[b] Vladimir L. Malinovskii,[a] and Robert Häner*[a]

Abstract: The electronic absorption, fluorescence, and excitation spectra of furo[3,4-*c*]furanone (**1**) have been measured in different solvents at different concentrations. We observed a complex dependence of absorption and excitation spectra as a function of the concentration in CH_2Cl_2 and THF due to aggregate formation. Interestingly, the fluorescence spectra were not affected. Resolving the puzzle was made possible by the fact that **1** fits perfectly into the channels of zeolite L (ZL) microcrystals to form **1**–ZL guest–host composites. The geometry of the ZL channel system ensures a well-defined orientation of the embedded dye molecules, thereby leading to a preferred orientation of their electronic transition dipole moment (ETDM) and thus to objects with pronounced optical anisotropy properties. This enabled us to understand that in solution the monomers that are present at low concentration form an aggregate in which the molecules sit on top of each other and arrange into a J-type aggregate configuration at higher concentrations. The signature of the latter is observed in the **1**–ZL composites. This seems to be the first example in which the insertion of molecules into a nanochannel microcrystal has helped in understanding the weak intermolecular interactions that take place in solution.

Keywords: aggregates · host–guest systems · nanochannels · supramolecular chemistry · zeolites

Introduction

Diaryl diketopyrrolopyrroles (DPPs) have found widespread use as technical pigments and dyes.[1–3] DPPs, as well as their oxygen analogues the difurofuranones (DFFs),[4,5] are also promising for use as components in electronic devices.[6,7] In our work directed towards the synthesis of natural-product-like polycyclic compounds,[8–11] we found that diaryl furofuranones such as **1** are readily accessible from furopyranone precursors.[12] Due to their obvious structural similarity to the DFFs, we subsequently investigated the spectroscopic properties of this new class of chromophores. Preliminary experiments indeed indicated notable parallels between the DPPs and DFFs, including high absorptivity and fluorescence with a Stokes shift that increases along with solvent polarity. Closer inspection revealed a complex dependence of absorption and excitation spectra as a function of the concentration in CH_2Cl_2 and THF due to aggregate formation. Interestingly, the fluorescence spectra were not affected. Resolving the puzzle was made possible by the fact that **1** fits perfectly into the channels of zeolite L (ZL).[13] The geometry of the ZL channel system ensures a well-defined orientation of the embedded dye molecules, thereby leading to a preferred orientation of their electronic transition dipole moment (ETDM) and thus to objects with pronounced optical anisotropy properties.[14] Comparison of the spectroscopic properties of **1** in solution at different concentrations and of **1**–ZL host–guest samples enabled us to understand that in solution, the monomers, which are present at very low concentration, form aggregates in which the molecules sit on top of each other. They then arrange into a J-type aggregate configuration at higher concentrations. We report the first example in which insertion of molecules into a nanochannel host helped in understanding processes in solutions.

[a] Prof. Dr. G. Calzaferri, Dr. T. Meng, Dr. V. L. Malinovskii, Prof. Dr. R. Häner
Department of Chemistry and Biochemistry
University of Bern, Freiestrasse 3, 3012 Bern (Switzerland)
Fax: (+41) 316318057
E-mail: gion.calzaferri@iac.unibe.ch
robert.häner@ioc.unibe.ch

[b] Dr. D. Brühwiler, Dr. L.-Q. Dieu
Institute of Inorganic Chemistry, University of Zürich
Winterthurerstrasse 190, 8057 Zürich (Switzerland)
Fax: (+41) 446356802
E-mail: bruehwi@aci.uzh.ch

Supporting information for this article is available on the WWW under http://dx.doi.org/10.1002/chem.201000728.

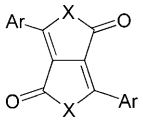

DPP: X = NH
DFF: X = O

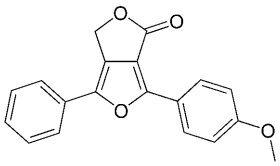

1

Results and Discussion

Absorption and fluorescence spectra in solution: The electronic absorption, fluorescence, and excitation spectra of **1** have been measured in different solvents at different concentrations. Shape and band positions of the absorption spectra of diluted solutions are nearly the same in solvents of different polarity and proton strength. This is illustrated in Figure 1, which shows spectra in THF, MeOH, CH_2Cl_2, and toluene. The value of the extinction coefficient at 358 nm in THF is 30000 $M^{-1}cm^{-1}$. It was determined at different concentrations in the range of 10^{-6} to 5×10^{-6} M, in which the Beer–Lambert law is fulfilled. The excitation spectra correspond to the absorption spectra as seen in Figure 2A. The fluorescence spectra measured in diluted solutions (10^{-6} M) show a considerable Stokes shift in all solvents, only moderate dependence on solvent polarity and refractive index, and they do not deviate much from mirror symmetry (Figure 2B). They are independent of excitation wavelength. Well-developed vibrational structure is displayed in *n*-hexane. Three vibrational bands and a shoulder

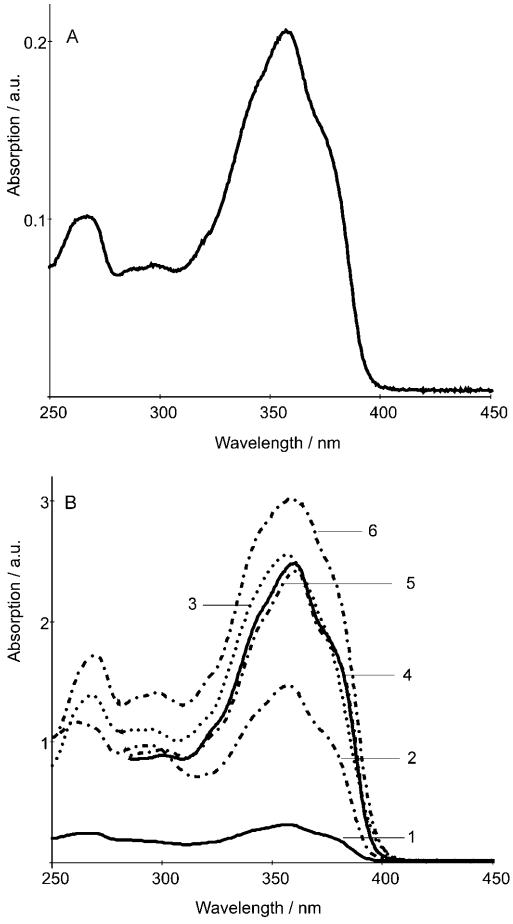

Figure 1. A) Electronic absorption spectrum of **1** in 1.5×10^{-5} M THF at RT. B) Comparison of the absorption spectra of **1** measured in different solvents and different conditions: 1) 10^{-4} M, THF, RT; 2) 5×10^{-4} M, THF, RT; 3) 10^{-3} M, MeOH, RT; 4) 10^{-3} M, CH_2Cl_2, RT; 5) 10^{-3} M, toluene, RT; and 6) 10^{-3} M, toluene, measured at 5 °C.

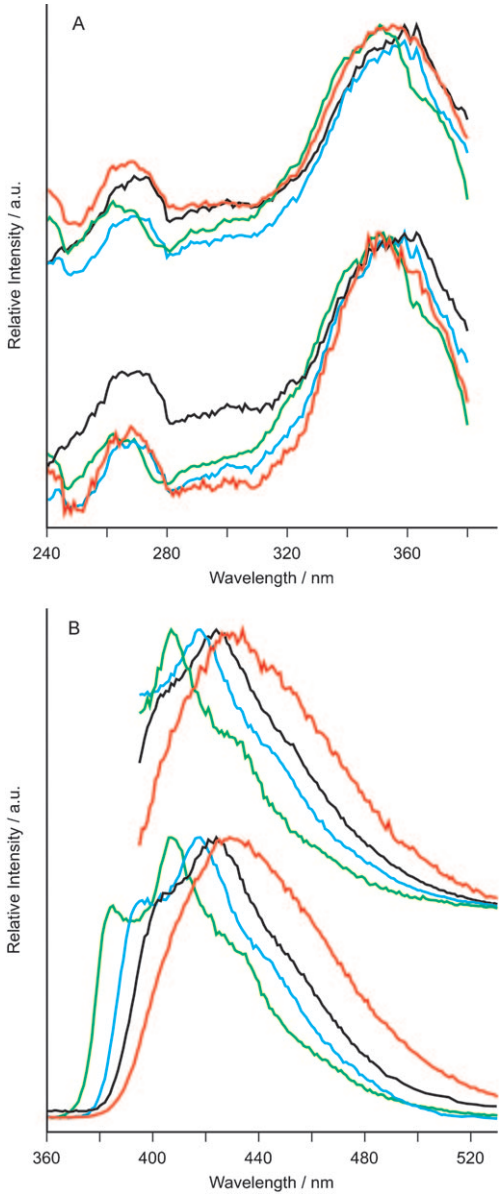

Figure 2. Excitation and fluorescence spectra, scaled to the same height at the maxima, of diluted solutions (10^{-6} M) of **1** in different solvents: A) Excitation spectra observed at 390 (lower group) and 450 nm (upper group): 1) CH_2Cl_2 (black), 2) THF (blue), 3) *n*-hexane (green), and 4) MeOH (red). B) Fluorescence spectra excited at 270 (lower group) and 385 nm (upper group): 1) CH_2Cl_2 (black), 2) THF (blue), 3) *n*-hexane (green), and 4) MeOH (red). The spectra measured upon excitation at 270 and 385 nm superimpose so well that hardly any difference can be seen.

are seen. These features disappear to a large extent in solvents of higher polarity, a behavior that is common for many organic molecules. The bathochromic shift correlates with the solvent polarity and the refractive index as anticipated by the Lippert–Mataga theory.[15] The data indicate that the geometry of **1** is little affected by the solvent in the electronic ground state S_0, but that considerable relaxation takes place in the electronically excited state S_1 in all solvents. The latter effect becomes more pronounced with an increase in solvent polarity.

We were surprised to observe a pronounced concentration dependence of the excitation spectra of **1** in THF and CH_2Cl_2 at concentrations above 10^{-5} M, because this was not expected on the basis of the data reported so far as well as what has been known from literature for this kind of molecules. The spectrum suddenly splits in two new bands. We show this in Figure 3 for a 10^{-4} M solution of **1** in THF. At

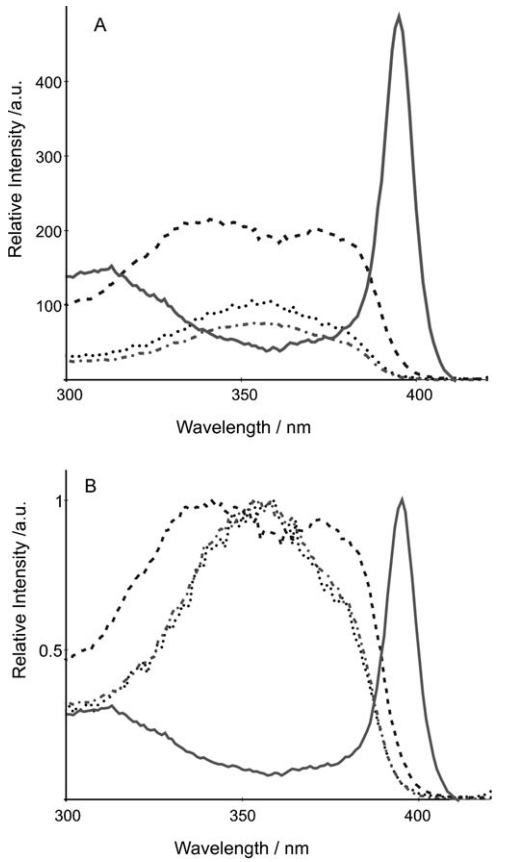

Figure 3. From monomers to aggregates in solutions of **1** in THF: A) Excitation spectra observed at 480 nm: 1) 10^{-6} (–·–·), 2) 10^{-5} (·····), 3) 10^{-4} (-----), and 4) 10^{-3} M (——). B) Comparison by scaling the spectra to equal height at their maxima.

even higher concentrations above 10^{-4} M, a new sharp band appears at 396 nm. The three different spectra observed at low, medium, and high concentration cannot be superimposed. Figure 3B shows that there is no difference regarding the shape of the spectra 1 and 2. It is also clear that spectrum 3 is not a superposition of spectrum 1 plus 4. Numerical analysis supports this observation. The three different spectra 1, 3, and 4 are linearly independent. This means that they represent three different species, two of which must be aggregates. We name them M for monomer, MM for the first appearing aggregate, and J for the second.

The evolution from MM- to J-aggregates is shown in more detail in Figure 4A. The intensity of the two new

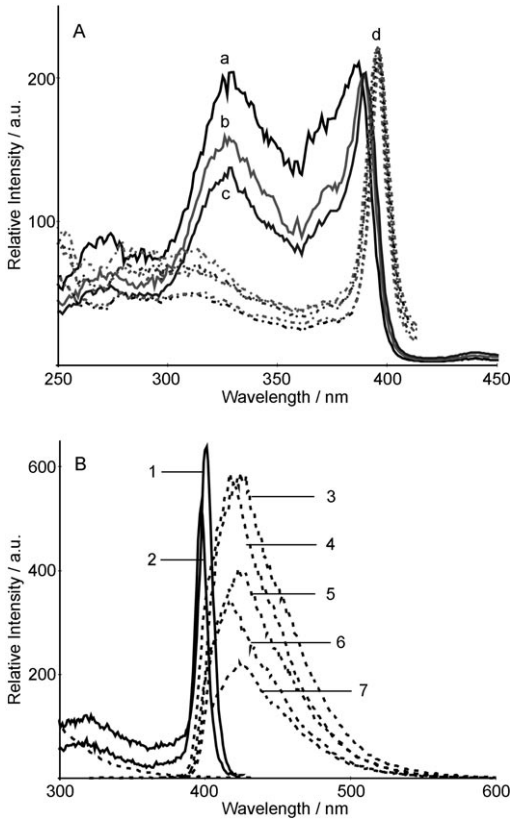

Figure 4. Excitation and luminescence spectra of aggregates formed by **1** at high concentrations: A) Excitation spectra observed at 480 nm in THF: a) 2×10^{-4} M, b) 3×10^{-4} M, c) 4×10^{-4} M, and d) 5×10^{-4}, 6×10^{-4}, 7×10^{-4}, 8×10^{-4}, and 9×10^{-4} M. B) Excitation spectra 1) and 2) observed at 480 nm and luminescence spectra 3)–7) excited at 310, 360, and 397 nm of 10^{-3} M solutions: 1) CH_2Cl_2 and 2) THF; 3) CH_2Cl_2, 310 nm; 4) THF, 310 nm; 5) CH_2Cl_2, 360 nm; 6) THF, 397 nm; and 7) CH_2Cl_2, 397 nm.

bands (a), with maxima at 329 and 387 nm, which characterize the MM-aggregates, is nearly the same at a concentration of 2×10^{-4} M and the band at 396 nm is not yet seen. This changes with an increase in concentration as seen in spectrum (b) and becomes even more pronounced in (c) in which the 329 nm band does not change position but becomes less important with respect to the longer wavelength feature. The latter appears to be shifted to a longer wavelength because the new J-aggregate band mixes in. At a concentration of 5×10^{-4} M, the spectrum that represents MM has disappeared and only the sharp 396 nm band (d) is visible. We show the spectra measured at concentrations of 5×10^{-4}, 6×10^{-4}, 7×10^{-4}, 8×10^{-4}, and 9×10^{-4} M scaled to the

same height at the maximum. No further dependence of the shape of the spectrum is observed once the sharp band at 396 nm has been developed. The properties of this band have been further examined by comparing the shape in CH_2Cl_2 and THF and by comparing the fluorescence spectrum upon excitation at different wavelengths. No important difference was observed with regards to the shape of either the excitation or the emission spectra by changing these parameters, as can be seen in Figure 4B.

The appearance of the 396 nm band at high concentrations of solutions of **1** in THF and CH_2Cl_2 is reminiscent of what has been often observed, especially for cyanine dyes, and has been interpreted as J-aggregate formation.[16,17] The remarkable change in the electronic absorption spectra caused by this kind of aggregate formation has been understood as being caused by ETDM coupling between resonant states of two or more chromophores.[18,19] The interaction depends on the relative orientation between the ETDM of the involved species, explained in Scheme 1. The weak resonance interaction between excited and unexcited molecules can lead to exciton splitting of excited states, which we denote as (M*···M)↔(M···M*), thus resulting in the appearance of new absorption bands. The magnitude of interactions β_C caused by exciton coupling, and hence the resulting splitting of the levels, depends on the oscillator strength f, the relative orientation κ, and the distance R between the interacting ETDM. It further depends on the $S_0 \rightarrow S_1$ electronic excitation energy ΔE, and on the refractive index n of the environment, as expressed in Equations (1) and (2):

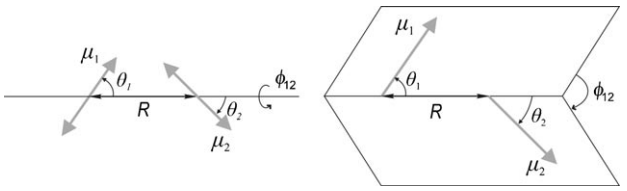

Scheme 1. Angles that describe the relative orientation of the ETDM μ_1 and μ_2 of two molecules. Left: representation of the ETDM as oscillators. Right: vector representation of the ETDM.

$$\beta_C = AD\frac{f}{\Delta E}\frac{\kappa}{R^3}\frac{1}{n^2} \quad (1)$$

$$\kappa = \sin\theta_1\sin\theta_2\cos\phi_{12} - 2\cos\theta_1\cos\theta_2 \quad (2)$$

The value of the constant AD is equal to $1.615\times 10^{-18}\,m^2cm^{-1}$ if we express β_C in cm^{-1}, which is convenient. This equation is valid for the interaction between two ETDM if their separation is large with respect to their length. The theory can easily be generalized for three or more interacting chromophores.[19,20] The most often discussed situations are those in which the interacting ETDM are in a plane ($\phi_{12}=0$) and in which θ_1 and θ_2 are equal. This situation is explained in Figure 5, which shows that the interaction β_C is largest for inline or collinear orientation of

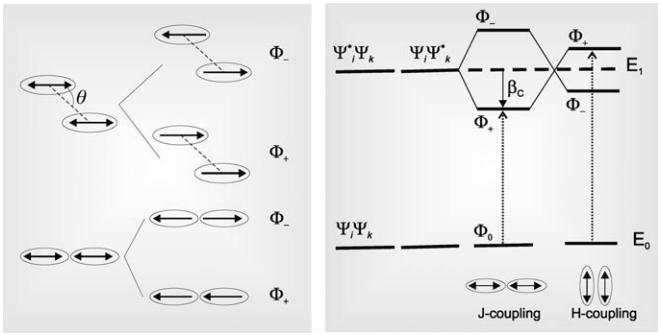

Figure 5. Phase-relation and energy-level diagram for ETDM interaction between the electronically excited state configurations $(M_i^*\cdots M_k)\leftrightarrow(M_i\cdots M_k^*)$. Left: diagram that shows the phase relation of the wave functions that describe the interaction caused by the ETDM. Right: energy-level diagram that shows the exciton splitting of two chromophores. The wave functions that describe the states in absence of any interaction are denoted as $\Psi_i\Psi_k$, $\Psi_i^*\Psi_k$, and $\Psi_i\Psi_k^*$, whereas the states induced by the interaction are denoted as Φ_0, Φ_+, and Φ_-. The interaction causes only a splitting of electronically excited states but has no consequences on the ground state. The different splitting of the excited-state levels for ETDM oriented inline or parallel, as represented by means of double arrows, is due to the angle dependence of κ. The allowed electronic transitions are indicated by the dotted arrows.[19,21]

the ETDM and changes sign if they are parallel. Collinear assembly leads to J- and parallel to H-coupling. The corresponding array of chromophores is usually designated as J-aggregates and H-aggregates, respectively. Crossing of the Φ_+ and Φ_- states occurs when $\cos^2(\theta)$ is equal to $^1/_3$. The transition $\Phi_0\rightarrow\Phi_+$ is allowed, whereas $\Phi_0\rightarrow\Phi_-$ is forbidden. This means that the formation of J-aggregates is manifested by a new band that appears at longer wavelengths, whereas the formation of H-aggregates causes a new band at shorter wavelengths. Both are accompanied by a decrease of the original $S_0\rightarrow S_1$ absorption band because the monomer M is used up.

The new sharp 396 nm band fits well with the interpretation of it being due to J-aggregate formation. The splitting observed at medium concentration, however, could only be understood based on Figure 5 if both transitions $\Phi_0\rightarrow\Phi_+$ and $\Phi_0\rightarrow\Phi_-$ were allowed, which is not the case. Configurations in which the interacting ETDM are not in a plane, which means $\phi_{12}\neq 0$, must be taken into account, because then situations exist in which both transitions are allowed. Assuming this, we can envisage processes as illustrated in Scheme 2 taking place. This means that we imagine that the

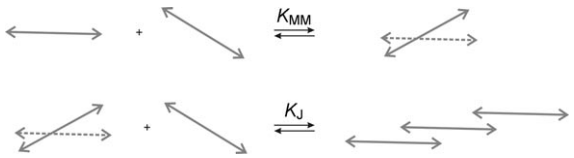

Scheme 2. Aggregate equilibrium. Upper: two of the nonsymmetrical monomers M form an aggregate MM. Lower: at higher concentrations an additional M is added to MM, thereby forming an aggregate J in which the ETDM are collinear.

three specific types of excitation spectra observed in THF and CH_2Cl_2 are due to equilibria between monomers M and two different types of aggregates. The ETDM are not in a plane for the first appearing species MM, whereas they are collinear for the J formed at higher concentrations. This is the simplest possible hypothesis we can make. It implies that at medium concentration two monomers M form an aggregate MM in which the ETDM, indicated in Scheme 2 as double arrows, are not in a plane. At higher concentrations an additional M is added to MM. The structure of the molecule is, however, such that MM can only grow if the molecules arrange in a way so that the ETDM become collinear.

These equilibria can be described by means of Equation (3), in which K_{MM} and K_J are the equilibrium constants and c_0 is the total amount of M dissolved, expressed in $mol\,L^{-1}$ (M). The parameter $[a_0]$ is equal to 1 M. It makes sure that the equilibrium constants are dimensionless. We must add it because we use concentrations and not activities.

$$\begin{aligned} &M + M \rightleftharpoons MM && K_{MM} = \frac{[MM]}{[M]^2}[a_0] \\ &M + MM \rightleftharpoons J && K_J = \frac{[J]}{[MM][M]}[a_0] \\ &c_0 = [M] + 2[MM] + 3[J] \end{aligned} \tag{3}$$

To find out if this hypothesis is consistent with the observations, we can solve Equation (3) for the concentrations [J], [MM], and [M] as reported in Equation (4).

$$\begin{aligned} &[J] + [J]^{\frac{2}{3}}\frac{2}{3}\left(\frac{K_{MM}}{K_J^2}[a_0]\right)^{\frac{1}{3}} + [J]^{\frac{1}{3}}\frac{[a_0]^{\frac{2}{3}}}{3(K_J K_{MM})^{\frac{1}{3}}} - \frac{c_0}{3} = 0 \\ &[MM] = [J]^{\frac{2}{3}}\left(\frac{K_{MM}}{K_J^2}[a_0]\right)^{\frac{1}{3}} \\ &[M] = c_0 - 2[MM] - 3[J] \end{aligned} \tag{4}$$

It is clear that K_{MM} must be larger than K_J because otherwise the sharp band at 396 nm would appear first; and it is also clear that K_{MM} is expected to be on the order of the magnitude of the concentration at which the double band, characteristic for the formation of MM, appears. Calculations have been made by using $K_{MM} = 10^4$ and $K_J = 0.4\,K_{MM}$ for a large total concentration c_0 range starting at 10^{-6} M, in which we know that the concentration of aggregates is negligibly small. Results are shown in Figure 6. We observe that the concentration of M changes at the beginning nearly linearly with an increase in c_0 but then starts to level off. At 10^{-5} M, the concentration of MM is already significant, and becomes larger than that of M above 7×10^{-5} M at which the concentration of J has also already grown considerably. The latter becomes dominant at about 5×10^{-4} M. This is in qualitative agreement with the data reported in Figures 3 and 4.

Equation (3) can be extended to the more general case expressed as follows [Eq. (5)]:

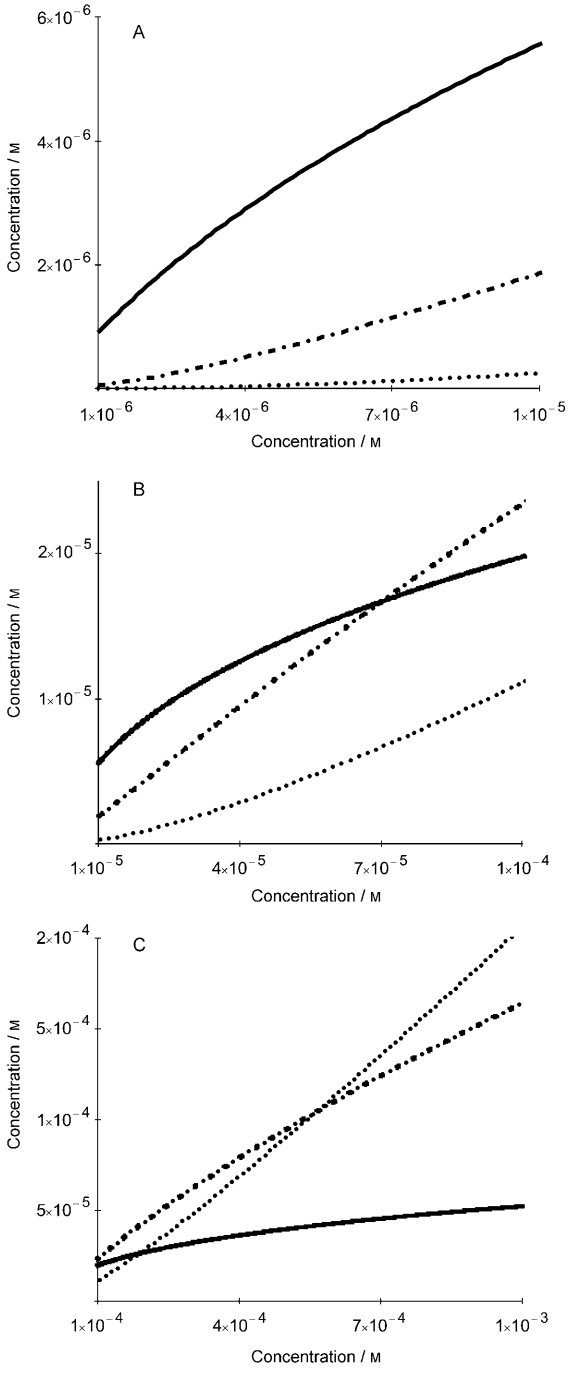

Figure 6. Numerical evaluation of the equilibria in Equation (3) with $K_{MM} = 10^4$ and $K_J = 0.4K_{MM}$. Concentration of monomer M (solid) and of the aggregates MM (dash-dot) and J (dotted) are reported as a function of the total amount c_0 of dissolved M. A) c_0 in the 10^{-6} M range. B) c_0 in the 10^{-5} M range. C) c_0 in the 10^{-4} M range.

$$\begin{aligned} &nM \rightleftharpoons Mn && K_{Mn} = \frac{[Mn]}{[M]^n}[a_0]^{n-1} \\ &mM \rightleftharpoons Jm && K_{Jm} = \frac{[Jm]}{[M]^m}[a_0]^{m-1} \\ &c_0 = [M] + n[Mn] + m[J] \end{aligned} \tag{5}$$

A general solution in terms of the concentrations [M], [Mn], and [Jm] can be derived similarly as reported above. Using $n=2$ and $m=3$, we find the situation reported by Equations (3) and (4), with $K_{MM}=K_{M2}$ and $K_{J3}=K_{MM}K_J$. Nothing of importance with respect to the problem we want to solve changes by extending the numbers n and m of involved species, only the discrimination would become even more pronounced.

Excitation and fluorescence spectra in a confined medium: The data and the reasoning reported so far support the interpretation of the concentration-dependent process proposed in Scheme 2. Confidence could be gained by means of an experiment, in which the formation of one of the two types of aggregate, MM or J, could be suppressed because of steric reasons. The influence of steric confinement has been explored in much detail.[14,20–25] ZL crystals provide hexagonally ordered one-dimensional nanochannels with a free diameter of 0.71 nm and a largest diameter of 1.26 nm. The length of a unit cell is 0.75 nm.[13] The geometry of the ZL channel system ensures the defined orientation of the embedded dye molecules, thereby leading to a characteristic orientation of the ETDM and thus to crystals with pronounced optical anisotropy properties.[21,25,26] The shape and size of **1** is such that it would fit well into the channels of ZL where it could stack in collinear arrangement of the ETDM. It would, however, be too bulky for the MM configuration as can easily be deduced from a simple van der Waals model. This means that we can expect that situations as schematically illustrated in Scheme 3 can be realized, in which we see on the left side two molecules that are so far apart that they behave as monomers, whereas on the right side two of them are so close that coupling of the ETDM becomes important. J-aggregate coupling of some dyes in the nanochannels of zeolite L has recently been observed.[21,27]

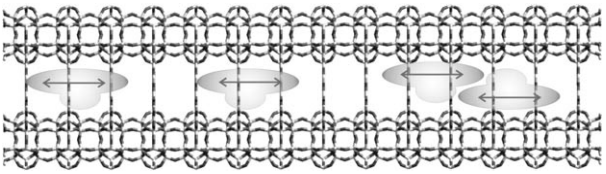

Scheme 3. Illustration of dye molecules in a ZL channel. Left: noninteracting molecules. Right: stacking that occurs at higher dye loading. The orientation of the ETDM is indicated as a double arrow.

Following this idea, we found that **1** can be inserted into the channels of ZL from the gas phase under mild conditions. The obtained material is stable in air and handling is therefore convenient. Easy substitution by water, which is a common phenomenon for nonpolar, neutral dyes like biphenyl, terphenyl, anthracene, and many others,[28] is not observed. This is most probably due to interaction of the carbonyl group with the potassium cations in the channel, as has recently been reported for fluorenone.[29] Only part of the ZL volume, namely, the large channels, is available for the guest species. It is convenient to introduce a parameter that provides information on dye concentration but is based on purely geometrical (space-filling) properties of ZL as a host (i.e., showing to which extent the ZL channels are filled with dye molecules). The loading, or occupation probability (p) of a dye–ZL material is defined in Equation (6):[14]

$$p = \frac{\text{number of occupied sites}}{\text{total amount of sites}} \tag{6}$$

The number of unit cells that a given dye occupies is usually, but not necessarily, an integer. It is equal to 2 in the present case, because the length of a unit cell is 0.75 nm and the van der Waals length of **1** is about 1.4 nm The loading p can range from 0 for an empty ZL to 1 if every site is occupied by one molecule. The dye concentration $c(p)$ of a **1**–ZL material in mol L^{-1} can be expressed as follows [Eq. (7)]:[14]

$$c(p) = 0.376\ (\text{mol L}) \times p \tag{7}$$

We show in Figure 7 a comparison of the excitation and emission spectra of a 10^{-6} M solution of **1** in THF and in ZL at a loading of $p=0.01$. The excitation maximum is at approximately the same wavelength in both media. This observation is in agreement with the data reported in Figures 1 and 2 in which we have seen that the absorption and excitation spectra of diluted solutions of **1** are little affected by the solvent. This fact very much facilitates interpretation of the data. The Stokes shift in THF is about -5000 cm^{-1} (75 nm). It is -7000 cm^{-1} (100 nm) in ZL and therefore comparable to that observed in MeOH (see Figure 2). The shape of the emission band in MeOH and in ZL is very similar.

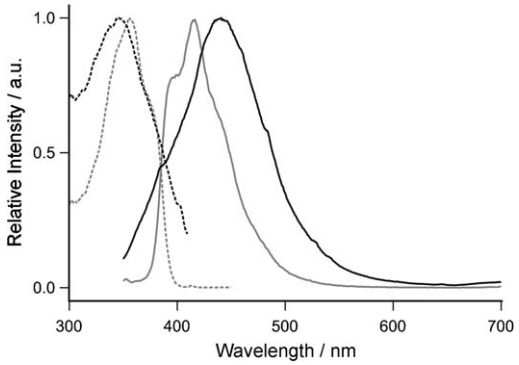

Figure 7. Electronic spectra of highly diluted **1**: Excitation (dashed, measured at 470 nm) and emission (solid, excited at 320 nm) spectra of **1** in THF (gray) and in ZL (black).

Fluorescence microscopy images of individual dye–ZL crystals allow for the determination of the orientation of the ETDM of dyes inside the channels and have been shown to

be an important tool for understanding such systems.[21,25,27,30,31] We therefore report polarized fluorescence microscopy images of **1**–ZL in Figure 8 for crystals with a loading $p=0.1$ and a length of about 2 μm. They show that the ETDM of **1** is aligned nearly parallel to the channel axis. This means that it should be possible to realize a packing as shown on the right side of Scheme 3.

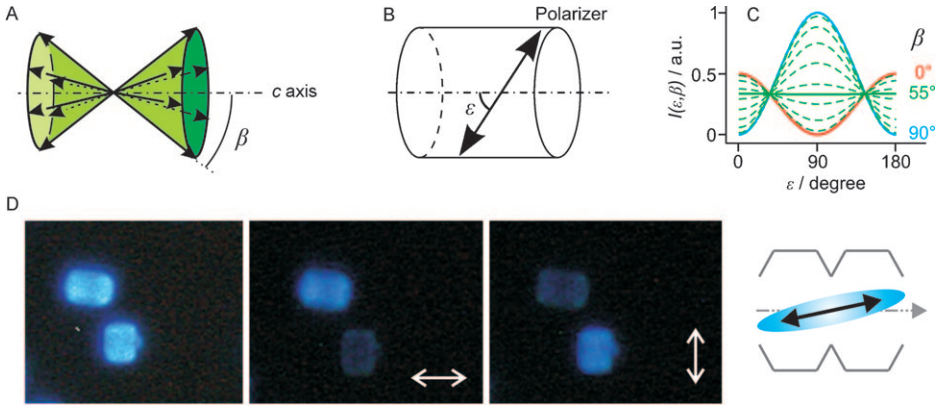

Figure 8. Orientation of ETDM of **1** inside the channels of ZL: A) Distribution of the ETDM on a double cone with a half-opening angle β. B) Polarization of emission observed when a single crystal is examined by means of a polarizer. C) Relative intensity of the observed fluorescence as a function of the observation angle ε with respect to the c axis, for different half-cone angles β. D) Orientations of the ETDM of **1**–ZL. Not polarized (left) and polarized (middle and right) fluorescence-microscope images of **1**–ZL crystals of about 2 μm length ($p=0.1$). The sample was excited at 330–385 nm and detected with a 420 nm cut-off filter. The direction of the polarizer is indicated by a double arrow. The scheme on the right shows the resulting orientation of the ETDM of **1**.

Figure 9 shows excitation and emission spectra of four **1**–ZL samples of different loading, $p=0.01$, 0.1, 0.27, and 0.47. We observe in Figure 9A and B that a new absorption band with a maximum at about 400 nm develops with an increase in loading but that the emission spectra are hardly affected. They show a moderate redshift, which is caused by self-absorption and therefore mainly seen when comparing the spectra of the $p=0.01$ and 0.1 samples. It is remarkable that the shape of the emission spectra is the same at 293 and at 77 K and independent of the excitation wavelength; only the emission intensity increases at

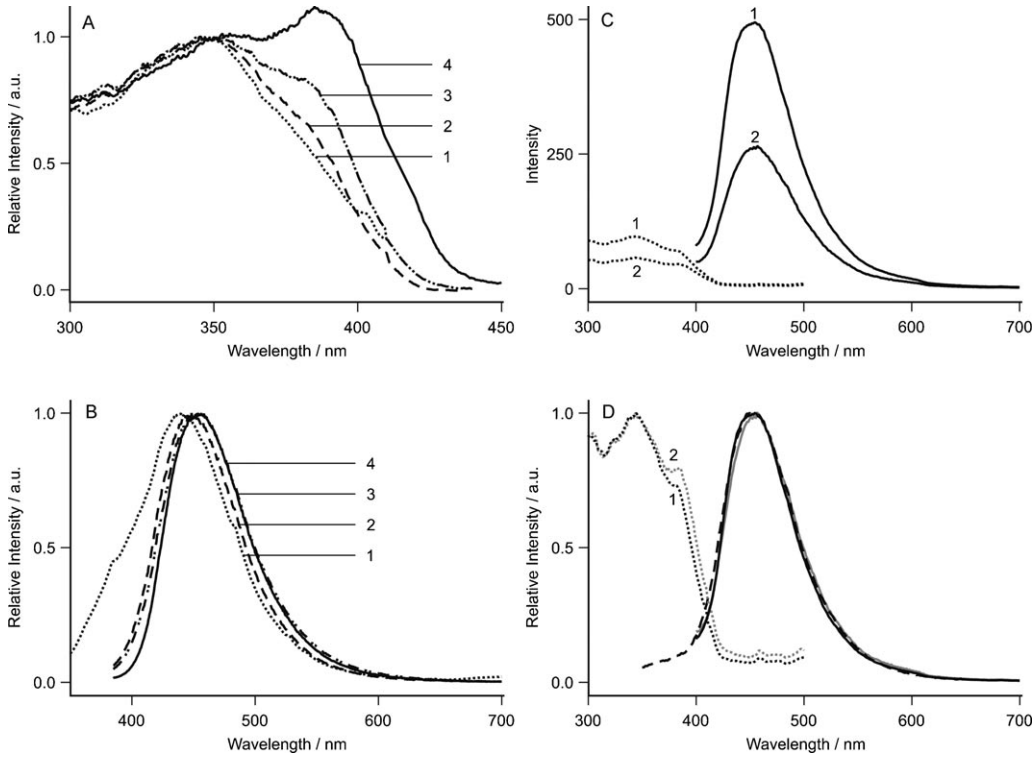

Figure 9. Excitation and emission spectra of **1**–ZL observed at different loadings and different temperatures: A) Excitation and B) emission spectra measured at different dye loadings: 1) $p=0.01$ (dotted); 2) $p=0.1$ (dashed); 3) $p=0.27$ (dashed-dotted); (4) $p=0.47$ (solid). C) Excitation (dotted, recorded at 550 nm) and emission (solid, excited at 380 nm) spectra of **1**–ZL ($p=0.26$) measured at 1) 77 K and at 2) room temperature. (D) The same as (C) but the spectra have been scaled to the same height at their maxima. In addition, an emission spectrum observed after excitation at 320 nm (gray) and measured at 293 K has been added. The three emission spectra are so similar that hardly any difference can be seen.

lower temperature. The new band in Figure 9A is shown as difference spectra in Figure 10: spectrum (1) was subtracted from the spectra (2), (3), and (4). The result obtained for

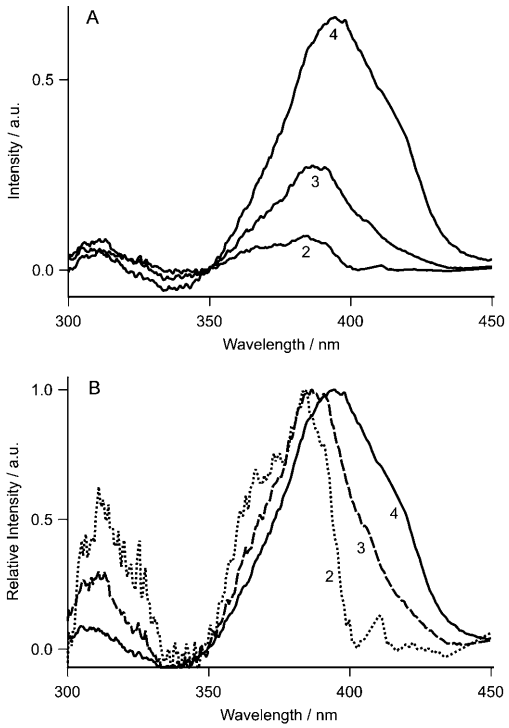

Figure 10. A) Difference spectra of **1**–ZL obtained by subtracting the excitation spectrum with $p=0.01$ from the excitation spectra of samples with 2) $p=0.1$, 3) $p=0.27$, and 4) $p=0.47$. B) The spectra are scaled to the same height at their maximum.

the $p=0.1$ sample is noisy because the new band is weak. It then, however, progresses rapidly into a well-shaped band at $p=0.27$ and becomes more intense at higher loading. The feature at about 310 nm remains unchanged. The development of the shape is better seen in the spectra that have been scaled to the same height at the maxima. The well-grown band at $p=0.47$ shows some broadening and is slightly redshifted with respect to the J-band in solution; see Figures 3 and 4 .

Conclusion

The weak influence of the solvent on the absorption spectra of diluted solutions of **1**, the near mirror symmetry of the excitation and fluorescence spectra in *n*-hexane, which is still present in THF and even in ZL, and the large oscillator strength of $f=0.57$ indicate that the first intense electronic absorption band at about 360 nm is of π–π* type. This is in agreement with molecular-orbital calculations. The AM1-optimized structure of **1** is shown in Scheme 4, in which we also indicate the orientation of the ETDM.[32] Up to 8×8 configurations have been included for calculating the electronic transitions. The absorption maximum of the first electronic transition is at 391 nm with oscillator strength 0.6. This corresponds well with the experimental observation. Configuration interaction turned out to be of minor importance, which means that the first absorption band can be understood essentially as a HOMO-to-LUMO transition. From this we conclude that the electronic absorption band and the fluorescence band of diluted solutions of **1** and also of **1**–ZL at low loading is of $S_0 \rightarrow S_1$, $\pi \rightarrow \pi^*$ and of $S_1 \rightarrow S_0$, $\pi^* \rightarrow \pi$ type, respectively. The length of the ETDM l_{μ^*} is equal to 0.136 nm as can be calculated by means of Equation (8), in which ΔE is equal to the energy of the transition in cm^{-1}:[20]

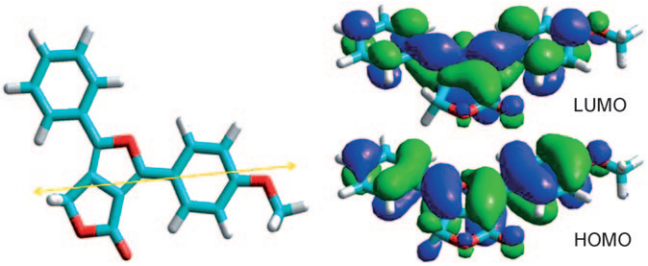

Scheme 4. AM1-optimized structure of **1** and orientation of the ETDM, indicated as a yellow double arrow, of the $S_0 \rightarrow S_1$ π–π* transition. On the right are the HOMO and the LUMO.

$$l_{\mu*} = 3.036 \times 10^{-6}\ \mathrm{cm}^{0.5} \sqrt{\frac{f}{\Delta E}} \qquad (8)$$

The exciton splitting β_C expected for a J-aggregate as a function of distance can be calculated by means of Equation (1). Results obtained for $\phi=0$, three different values of θ, and a refractive index of 1.4 are reported in Figure 11. The angle $\theta=0$ corresponds to an "ideal" J-aggregate situation and $\theta=\pi/2$ to an "ideal" *H* aggregate situation, as illustrated in Figure 5. The calculation for $\theta=\pi/6$ shows that small deviations from the "ideal" angle are of moderate influence on the magnitude of interaction. The splitting increases with the number of molecules that form the J-aggregate; see, for example, refs. [19] and [20]. We do not consider this explicitly but keep it in mind when comparing the calculated with the experimental data.

The position of the $S_0 \rightarrow S_1$ transition is at 358 nm, and the new sharp band appears at 396 nm, as seen in Figures 3 and 4. From this we find the experimental value $\beta_C(\mathrm{exptl}) = 2680\ \mathrm{cm}^{-1}$. Comparing this with the data reported in Figure 11 allows one to draw the conclusion that the ETDM distance in the J-aggregate is about 0.5 nm. To calculate the interaction β_C for the double band of the MM-aggregate, Figure 3, we need to know the angles ϕ_{12}, θ_1, and θ_2. We do not have this information but we know that ϕ_{12} is not zero, because otherwise only one of the two transitions would be allowed. The two transitions have, however, the same oscillator strength at angles: $\phi_{12}=\pi/4$ and $\theta_1=\theta_2=\pi/2$.[20,21] We further know that the MM-aggregate does not form in the

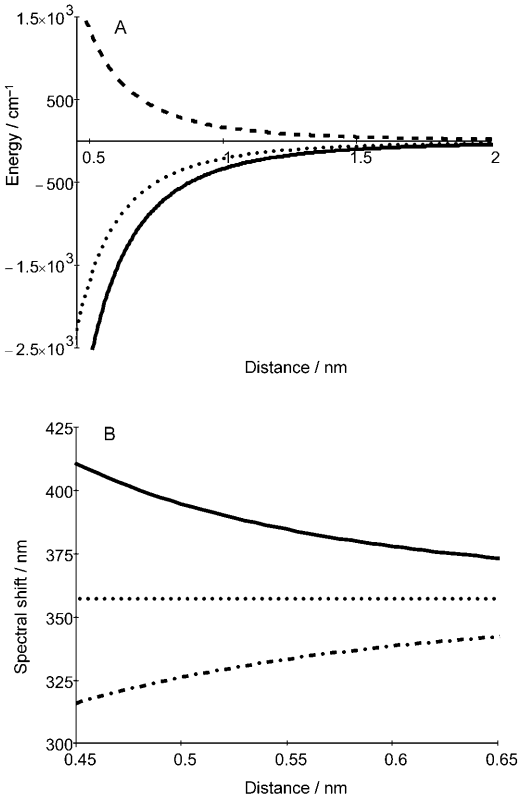

Figure 11. Exciton splitting: A) Magnitude of the interaction β_C as a function of separation of the ETDM obtained for $\phi=0$ and $\theta=0$ (solid), Bπ/6 (dotted), and $\pi/2$ (dashed). B) The solid line shows the bathochromic shift of the J-aggregate absorption band as a function of distance between the ETDM. The dotted line marks the wavelength of the $S_0 \rightarrow S_1$ transition and is used as reference. The dash-dotted line shows the position of the short wavelength J-aggregate band, which is, however, not seen in the experiment, because it is forbidden; see also Figure 5.

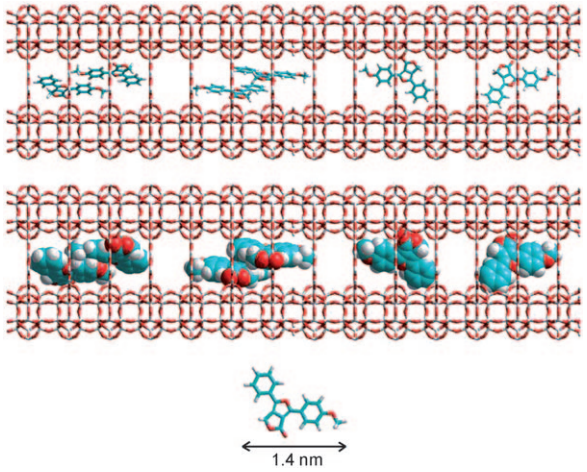

Figure 12. Molecule **1** in a channel of ZL. The length of **1** is about 1.4 nm. On the right we see two isolated molecules oriented with the ETDM parallel to the channel axis as deduced from the optical microscopy data reported in Figure 8. Three different combinations for J-aggregate coupling are possible, two of which are illustrated on the left.

ZL channels because the corresponding spectral signature has not been observed in any of the **1**–ZL samples we have investigated. This is in agreement with the drawing of the ETDM arrangement in Scheme 2. The spectral features and the luminescence microscopy images observed for **1**–ZL samples are consistent with noninteracting monomers at low loading, as illustrated on the right side of Figure 12. Two different ways are possible with the same probability, one with the methoxy group pointing to the right and one where it points to the left. This allows in principle three different combinations for J-aggregate coupling. We illustrate two of them in Figure 12.

The broadening of the J-aggregate band reported in Figures 9A and 10 may to some extent be caused by the fact that the spectra represent an average of a huge number of small crystals. The existence of three different arrangements, but also the fact that the average distance may become shorter with an increase in loading, can cause some broadening and bathochromic shift. Time, space, and spectrally resolved near-UV confocal microscopy excitation spectra of a representative selection of individual crystals—data that are still difficult to obtain—would be needed to check this hypothesis.[27b] In summary, we can conclude that the properties of the **1**–ZL samples support the interpretation schematically illustrated in Scheme 2. An intriguing question, however, remains: Why are the shape and position of the luminescence spectra independent of the loading, the excitation wavelength, and the temperature; and why are they always essentially the same independent of the concentration? The answer to this, consistent with all facts available, is that the Stokes shift for the fluorescence under all conditions we have investigated is larger, typically on the order of 80–100 nm or about 5000 cm^{-1}, than the shift due to J-aggregate coupling, which is on the order of 40 nm or about 2800 cm^{-1}. The consequence is that the excited Φ_+ state of the aggregates rapidly reaches the relaxed S_1 state of M, which is the lowest emitting state, and which emits in the same wavelength range, independently of whether or not it has been reached by direct excitation or by relaxation from the Φ_+ state. This is illustrated in Figure 13. It means that the energy-resonance condition, which must be fulfilled for observing $\Phi_+ \rightarrow S_0$ emission, is broken before this process can take place. The lack of symmetry of **1** is expected to favor this behavior because only little relaxation is needed to break the resonance condition.

Luminescence of J-aggregates is usually observed for dyes that show mirror symmetry and small Stokes shifts between absorption and emission. If the Stokes shift is larger than the bathochromic shift caused by J-aggregate coupling so that the relaxed state of the monomer is lower than that of the J-aggregate, as shown in Figure 13, then the system has the option to evolve rapidly into this lowest state. We conclude that the surprising observation of the pronounced concentration dependence of the excitation spectra of **1** in THF and CH_2Cl_2 at concentrations above 10^{-5} M, and the fact that the fluorescence spectrum is independent of concentration, are caused by the formation of aggregates of binding energy

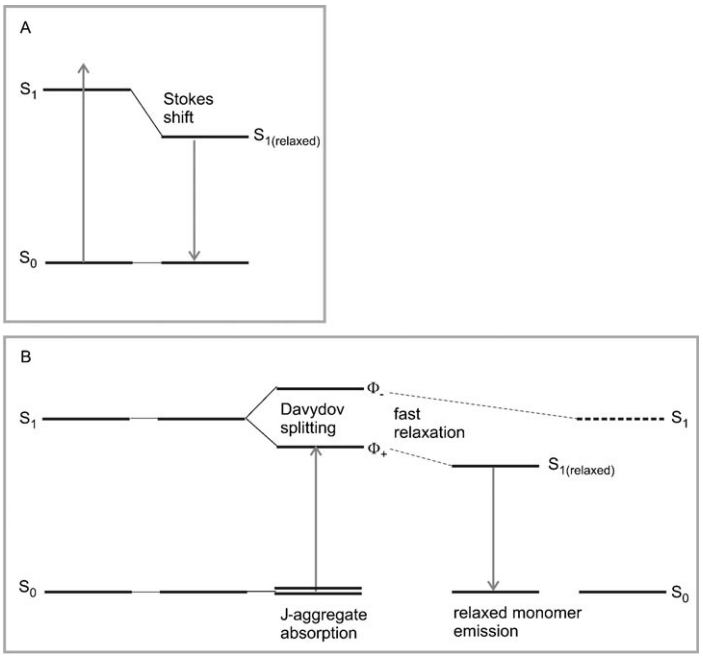

Figure 13. State diagram and relaxation processes. A) Energy-level diagram for fluorescence of a monomer with relaxation, thereby resulting in a large Stokes shift. B) Energy-level diagram of a J-aggregate, which suggests a relaxed monomer emission.

on the order of 20 kJ mol^{-1}, which change the relative orientation of the ETDM and hence their conformation upon growing from MM to J. Unambiguous interpretation was made possible by the fact that **1** can be inserted into the nanochannels of ZL and that it is small enough to enter the channels under mild conditions but too bulky for formation of H-type aggregates inside. The geometry of the ZL channel system thus ensures the defined orientation of the embedded molecules, thereby leading to a preferred orientation of the ETDM. This seems to be the first example in which the insertion of molecules into a nanochannel host material helped to understand weak intermolecular interactions that take place in solution. It will be interesting to see if more general methods for the elucidation of similar phenomena can be derived from this study.

Experimental Section

Compound **1**[12] and ZL[33] have been synthesized and characterized as reported previously. UV/Vis spectra were collected with an optic path of 1 cm over the range of 210–500 nm at 20 °C using a Varian Cary-100 Bio-UV/Vis spectrophotometer equipped with a Varian Cary block temperature controller. Fluorescence data were collected at 20 °C using a Varian Cary Eclipse fluorescence spectrophotometer equipped with a Varian Cary block temperature controller using 1×1 cm quartz cuvettes. All spectra were measured in spectroscopy-grade solvents.

Inclusion of **1** into K^+-exchanged zeolite L crystals[33] with a length of 1.2–2.8 μm and a diameter of 0.7–1.2 μm was performed by sublimation. A weighed amount of zeolite L and **1** was introduced into a glass ampoule. After vigorous vortexing, the mixed powder was dried at 80 °C in a vacuum for 16 h. The evacuated ampoule was sealed and heated to 165–170 °C in a rotating oven for 24–96 h. Long heating times were applied to maximize the loading. The material was washed several times with methanol to remove molecules adsorbed on the external surface of the crystals. Photoluminescence spectra of **1**–ZL (deposited on a quartz plate) were measured using a Perkin–Elmer LS50B spectrometer. For low-temperature measurements, the spectrometer was equipped with a nitrogen cryostat (Oxford Instruments PE 1704). Fluorescence microscopy images were recorded using an Olympus BX60 microscope and an Olympus SIS CC-12 CCD camera, which has a resolution of 196 nm for an emission at 450 nm; the numerical aperture is 1.4. Molecular-orbital and force-field calculations have been carried out using Hyperchem Professional, Release 8.04 software.

Acknowledgements

D.B. and L.-Q.D. acknowledge financial support by the Swiss National Science Foundation (grant 200020-117591) and by the European Commission through the Human Potential Programme (Marie-Curie RTN Nanomatch, grant no. MRTN-CT-2006-035884). R.H. gratefully acknowledges financial support by the Swiss National Foundation (grant 200020-117617).

[1] T. Potrawa, H. Langhals, *Chem. Ber./Recl.* **1987**, *120*, 1075–1078.
[2] A. Iqbal, M. Jost, R. Kirchmayr, J. Pfenninger, A. Rochat, O. Wallquist, *Bull. Soc. Chim. Belg.* **1988**, *97*, 615–643.
[3] Z. M. Hao, A. Iqbal, *Chem. Soc. Rev.* **1997**, *26*, 203–213.
[4] K. Zhang, B. Tieke, *Macromolecules* **2008**, *41*, 7287–7295.
[5] S. Lunak, Jr., J. Vynuchal, R. Hrdina, *J. Mol. Struct.* **2009**, *919*, 239–245.
[6] A. B. Tamayo, B. Walker, T. Q. Nguyen, *J. Phys. Chem. C* **2008**, *112*, 11545–11551.
[7] A. R. Rabindranath, Y. Zhu, I. Heim, B. Tieke, *Macromolecules* **2006**, *39*, 8250–8256.
[8] R. Messer, C. A. Fuhrer, R. Häner, *Curr. Opin. Chem. Biol.* **2005**, *9*, 259–265.
[9] R. Messer, X. Pelle, A. L. Marzinzik, H. Lehmann, J. Zimmermann, R. Häner, *Synlett* **2005**, 2441–2444.
[10] C. Fuhrer, R. Messer, R. Häner, *Tetrahedron Lett.* **2004**, *45*, 4297–4300.
[11] C. A. Fuhrer, E. Grüter, S. Ruetz, R. Häner, *ChemMedChem* **2007**, *2*, 441–444.
[12] T. Meng, C. A. Fuhrer, R. Häner, *Synlett* **2009**, 1951–1954.
[13] a) D. W. Breck, *Zeolite Molecular Sieves*, Wiley, New York, **1974**; b) International Zeolite Association, http://www.iza-structure.org/databases/; c) C. Baerlocher, W. M. Meier, D. H. Olson, *Atlas of Zeolite Framework Types*, 5th ed., Elsevier, Amsterdam, **2001**; d) T. Ohsuna, B. Slater, F. Gao, J. Yu, Y. Sakamoto, G. Zhu, O. Terasaki, D. E. W. Vaughan, S. Qiu, C. R. A. Catlow, *Chem. Eur. J.* **2004**, *10*, 5031; e) O. Larlus, V. P. Valtchev, *Chem. Mater.* **2004**, *16*, 3381; f) Y. Lee, C-C. Kao, S. J. Kim, H-H. Lee, D. R. Lee, T. J. Shin, J. Y. Choi, *Chem. Mater.* **2007**, *19*, 6252.
[14] G. Calzaferri, S. Huber, H. Maas, C. Minkowski, *Angew. Chem.* **2003**, *115*, 3860–3888; *Angew. Chem. Int. Ed.* **2003**, *42*, 3732–3758.
[15] J. R. Lakowicz, *Principles of Fluorescence Spectroscopy*, 3rd ed., Springer, New York, **2006**.
[16] a) R. Steiger, R. Pugin, J. Heier, *Colloids Surf. B* **2009**, *74*, 484–491; b) A. N. Lebedenko, G. Y. Guralchuk, A. V. Sorokin, S. L. Yefimova, Y. V. Malyukin, *J. Phys. Chem. B* **2006**, *110*, 17772–17775; c) *J-aggregates* (Ed.: T. Kobayashi), World Scientific, Singapore, **1996**; d) J. R. Lenhard, B. R. Hein, *J. Phys. Chem.* **1996**, *100*, 17287–17296; e) V. F. Kamalov, I. A. Struganova, K. Yoshihara, *J. Phys. Chem.* **1996**, *100*, 8640–8644.
[17] a) U. De Rossi, S. Daehne, S. C. Meskers, H. P. Dekkers, *Angew. Chem.* **1996**, *108*, 827–830; *Angew. Chem. Int. Ed. Engl.* **1996**, *35*, 760–763; b) X.-Q. Li, X. Zhang, S. Ghosh, F. Würthner, *Chem. Eur. J.* **2008**, *14*, 8074–8078.

[18] A. S. Davydov, *Usp. Fiz. Nauk* **1964**, *82*, 393–448.
[19] a) M. Kasha, H. R. Rawls, M. Ashraf El-Bayoumi, *Pure Appl. Chem.* **1965**, *11*, 371–392; b) E. G. McRae, M. Kasha in *Physical Progress in Radiation Biology*, Academic Press, New York, **1964**, pp. 23–42.
[20] a) G. Calzaferri, A. Devaux in *Supramolecular Effects in Photochemical and Photophysical Processes* (Eds.: V. Ramamurthy, Y. Inoue), Wiley, New York, in press; b) G. Calzaferri, *Nuovo Cimento* **2008**, *123B*, 1337–1367.
[21] G. Calzaferri, K. Lutkouskaya, *Photochem. Photobiol. Sci.* **2008**, *7*, 879–910.
[22] a) V. Ramamurthy, *Photochemistry in Organized and Constrained Media* (Ed.: V. Ramamurthy), VCH, Weinheim, **1991**, pp. 429–493; b) T. Bein in *Studies in Surface Science and Catalysis, Vol. 168: Introduction to Zeolite Chemistry*, 3rd ed. (Eds.: J. Cejka, H. van Bekkum, A. Corma, F. Schüth), Elsevier, Amsterdam, **2007**, pp. 611–658.
[23] a) G. Schulz-Ekloff, D. Wöhrle, B. van Duffel, R. A. Schoonheydt, *Microporous Mesoporous Mater.* **2002**, *51*, 91–138; b) S. Hashimoto, M. Hagari, N. Matsubara, S. Tobita, *Phys. Chem. Chem. Phys.* **2001**, *3*, 5043–5051; c) S. Hashimoto, *J. Photochem. Photobiol. C* **2003**, *4*, 19–49; d) M. N. Chrétien, *Pure Appl. Chem.* **2007**, *79*, 1–20; e) S. Huber, A. Zabala Ruiz, H. Li, G. Patrinoiu, Ch. Botta, G. Calzaferri, *Inorg. Chim. Acta* **2007**, *360*, 869–875; f) M. Tsotsalas, M. Busby, E. Gianolio, S. Aime, L. De Cola, *Chem. Mater.* **2008**, *20*, 5888–5893; g) A. M. M. Abeykoon, M. Castro-Colin, E. V. Anokhina, M. N. Iliev, W. Donner, A. J. Jacobson, S. C. Moss, *Phys. Rev. B* **2008**, *77*, 075333; h) S. Hashimoto, M. Yamaji, *Phys. Chem. Chem. Phys.* **2008**, *10*, 3124–3130; i) J. Zhu, Y. J. Huang, *J. Phys. Chem. C* **2008**, *112*, 14241–14246; j) M. Busby, H. Kerschbaumer, G. Calzaferri, L. De Cola, *Adv. Mater.* **2008**, *20*, 1614–1618; k) Y. Wang, H. Li, Yu Feng, H. Zhang, G. Calzaferri, T. Ren, *Angew. Chem.* **2010**, *122*, 1476–1480; *Angew. Chem. Int. Ed.* **2010**, *49*, 1434–1438.
[24] a) D. Brühwiler, G. Calzaferri, T. Torres, J. H. Ramm, N. Gartmann, L.-Q. Dieu, I. López-Duarte, M. V. Martínez-Díaz, *J. Mater. Chem.* **2009**, *19*, 8040–8067; b) G. Calzaferri, H. Li, D. Brühwiler, *Chem. Eur. J.* **2008**, *14*, 7442–7449.
[25] S. Megelski, A. Lieb, M. Pauchard, A. Drechsler, S. Glaus, C. Debus, A. J. Meixner, G. Calzaferri, *J. Phys. Chem. B* **2001**, *105*, 25–35.
[26] A. Gasecka, L.-Q. Dieu, D. Brühwiler, S. Brasselet, *J. Phys. Chem. B* **2010**, *114*, 4192–4198.
[27] a) M. Busby, C. Blum, M. Tibben, S. Fibikar, G. Calzaferri, V. Subramaniam, L. De Cola, *J. Am. Chem. Soc.* **2008**, *130*, 10970–10976; b) C. Blum, Y. Cesa, M. Escalante, V. Subramaniam, *J. R. Soc. Interface* **2009**, *6*, S35-S43; c) G. Calzaferri, L. De Cola, M. Busby, Ch. Blum, V. Subramaniam, UK0812218.6, US/PTO 12/361616.
[28] M. Pauchard, A. Devaux, G. Calzaferri, *Chem. Eur. J.* **2000**, *6*, 3456–3470.
[29] a) E. Fois, G. Tabacchi, G. Calzaferri, *J. Phys. Chem. C* **2010**, *114*, 10572–10579; b) A. Devaux, C. Minkowski, G. Calzaferri, *Chem. Eur. J.* **2004**, *10*, 2391–2408.
[30] M. Pauchard, S. Huber, R. Méallet-Renault, H. Maas, R. Pansu, G. Calzaferri, *Angew. Chem.* **2001**, *113*, 2921–2924; *Angew. Chem. Int. Ed.* **2001**, *40*, 2839–2842.
[31] S. Hashimoto, K. Samata, T. Shoji, N. Taira, T. Tomita, S. Matsuo, *Microporous Mesoporous Mater.* **2009**, *117*, 220–227.
[32] G. B. Rocha, R. O. Freire, A. M. Simas, J. J. P. Stewart, *J. Comput. Chem.* **2006**, *27*, 1101–1111.
[33] a) A. Zabala Ruiz, D. Brühwiler, T. Ban, G. Calzaferri, *Monatsh. Chem.* **2005**, *136*, 77–89; b) A. Zabala Ruiz, D. Brühwiler, L.-Q. Dieu, G. Calzaferri in *Materials Syntheses: A Practical Guide* (Eds.: U. Schubert, N. Hüsing, R. Laine), Springer, Wien, **2008**, pp. 9–19.

Received: March 23, 2010
Published online: August 19, 2010

